Journal of Minerals and Materials Characterization and Engineering, 2023, 11, 1-15
https://www.scirp.org/journal/jmmce
ISSN Online: 2327-4085
ISSN Print: 2327-4077

Synthesis and Characterization of Gadolinium Oxide-Hematite Magnetic Ceramic Nanostructures

Sarah Glasser[1], Andrew J. Craig[2], Felicia Tolea[3], Mihaela Sofronie[3], Jennifer A. Aitken[2], Monica Sorescu[1]

[1]Department of Physics, Duquesne University, Fisher Hall, Pittsburgh, PA, USA
[2]Department of Chemistry and Biochemistry, Duquesne University, Mellon Hall, Pittsburgh, PA, USA
[3]National Institute of Materials Physics, Bucharest-Magurele, Romania
Email: sorescu@duq.edu

How to cite this paper: Glasser, S., Craig, A.J., Tolea, F., Sofronie, M., Aitken, J.A. and Sorescu, M. (2023) Synthesis and Characterization of Gadolinium Oxide-Hematite Magnetic Ceramic Nanostructures. *Journal of Minerals and Materials Characterization and Engineering*, **11**, 1-15.
https://doi.org/10.4236/jmmce.2023.111001

Received: November 17, 2022
Accepted: December 27, 2022
Published: December 30, 2022

Abstract

Mixed-oxide nanostructures of the type xGd_2O_3-$(1-x)\alpha$-Fe_2O_3 (x=0.1, 0.3, 0.5 and 0.7) were synthesized by mechanochemical activation for ball milling times of 0, 2, 4, 8 and 12 hours. The systems were subsequently analyzed by Mössbauer spectroscopy, X-ray powder diffraction (XRPD), magnetic measurements and optical diffuse reflectance spectroscopy. The magnetic hyperfine field was studied as function of ball milling time for all sextets involved and found to be consistent with the formation of a limited solid solution in the systems investigated. The end-product was the gadolinium perovskite, represented by a doublet whose abundance was derived as function of the milling time. The XRPD patterns recorded for the equimolar composition were dominated by the diffraction peaks of $GdFeO_3$ after 12 hours of milling. The hysteresis loops were recorded at 300 and 5 K in an applied magnetic field of 5 T and were interpreted as a superposition of paramagnetic behavior of gadolinium oxide and weak ferromagnetic behavior of hematite and gadolinium perovskite. The Morin transition of hematite was inferred from zero-field-cooling-field-cooling (ZFC-FC) curves measured with a magnetic field of 200 Oe in the 5-300 K temperature range and was found to depend on the ball milling time. Optical diffuse reflectance spectra showed that the compounds were semiconductors with an optical band gap of 2.1 eV.

Keywords

Gadolinium Oxide, Hematite, Mössbauer Spectroscopy, Magnetic Properties, Optical Properties

1. Introduction

Hematite (α-Fe_2O_3) has been the subject of intense theoretical and experimental investigations due to its use as a magnetic, semiconductor and catalytic material [1]-[6]. Doping hematite with various transition metals and rare earth elements was found to result in an improvement of its electrochemical and photocatalytical properties [7]-[15]. On the other hand, the structural, dielectric, morphological and magnetic properties of Gd_2O_3 nanorods were investigated, both with and without Co dopants [16] [17] [18] [19]. Gadolinium perovskite, $GdFeO_3$ was found to have interesting low temperature magnetic properties and exhibit an enhancement of the magnetoelectric coupling when substituted with Mg [20]-[25].

The phase sequence in the Fe_2O_3-Gd_2O_3 mixed oxide nanoparticles system was discussed in [13] [14], while using co-precipitation as a synthetic method. In the present study, we investigate the structural, magnetic and optical properties of the xGd_2O_3-(1-x)α-Fe_2O_3 system with molar concentration x = 0.1, 0.3, 0.5 and 0.7, obtained by mechanochemical activation at different ball-milling times. Our investigation is conducted by Mössbauer spectroscopy, X-ray powder diffraction (XRPD), magnetic measurements (hysteresis loops and zero-field-cooling-field-cooling) and optical diffuse reflectance spectroscopy.

2. Materials and Methods

Nanoparticles of xGd_2O_3-(1-x)α-Fe_2O_3 (x = 0.1, 0.3, 0.5 and 0.7) were obtained by mechanochemical activation of precursor powders of hematite and gadolinium oxide with particle sizes of 50 and 90 nm, respectively (purity 99.9%, Alfa Aesar). The powders were introduced in a SPEX 8000 mixer mill and ground for time periods ranging from 0 to 12 hours. The powder to ball mass ratio was 1:5. Prior to introduction in the SPEX chamber, the powders were mixed manually using a mortar and pestle.

The room-temperature transmission Mössbauer spectra were recorded using a SeeCo constant accelerator spectrometer equipped with a 25 mCi ^{57}Co gamma-ray source in a Rh matrix. All spectra were analyzed by least-squares fitting using the WINORMOS package of programs in the assumption of Lorentzian lineshapes.

The powder diffraction patterns (XRPD) of the gadolinium oxide-hematite ball-milled samples were recorded with a Malvern Panalytical third generation Empyrean X-ray powder diffractometer system with CuKα radiation (λ = 1.54187 Å). An X'cellerator detector was used, with a diffraction angle 2θ of 10 - 80˚ and a preselected step size of 0.02˚. The diffraction peaks were identified using the powder diffraction file (PDF) cards for hematite, gadolinium oxide and gadolinium perovskite, respectively.

Magnetic property measurements were performed using a superconductor quantum interference device (SQUID)-Quantum Design magnetometer with a 5 T magnetic field for recording the hysteresis loops at 300 and 5 K and a 200 Oe

magnetic field for the zero-field-cooling-field-cooling (ZFC-FC) measurements in the 5 - 300 K temperature range.

Optical diffuse reflectance spectra were obtained using a Varian Cary 5000 UV/Vis/NIR spectrometer. The samples were loaded into a Harrick Praying Mantis diffuse reflectance accessory that used elliptical mirrors. $BaSO_4$ was used as a 100% reflectance standard. Scans were performed from 2500 to 200 nm at a rate of 600 nm/min, wavelength data were converted to electron volts, and the percent reflectance data were converted to absorbance units.

3. Results and Discussion

3.1. Mössbauer Spectroscopy

Figures 1(a)~(e)-4(a)~(e) show the room-temperature transmission Mössbauer spectra of the xGd_2O_3-(1-x)α-Fe_2O_3 nanoparticles system for molar concentration x

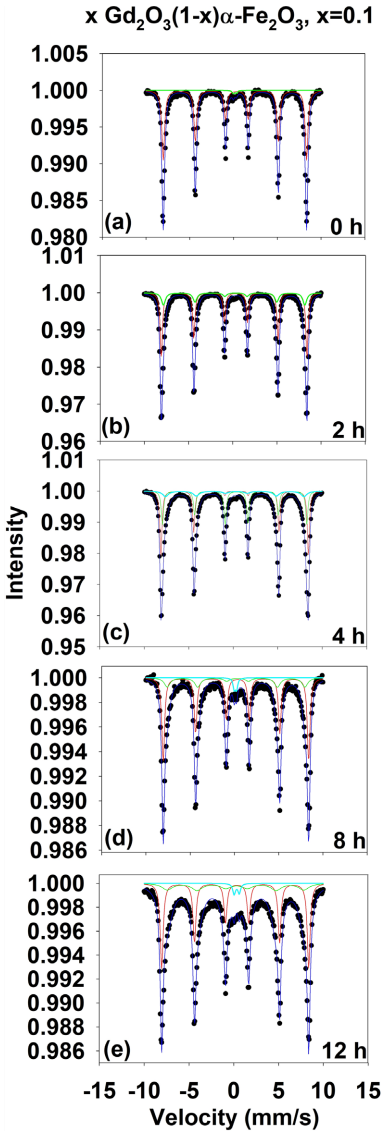

Figure 1. Mössbauer spectra for x = 0.1 at different milling times.

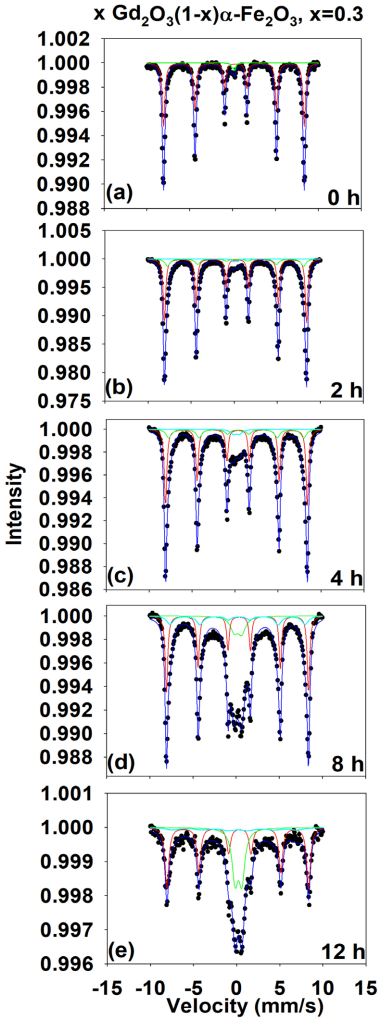

Figure 2. Mössbauer spectra for x = 0.3 at different milling times.

= 0.1, 0.3, 0.5, 0.7 and ball milling times (BMT) of 0, 2, 4, 8 and 12 hours, respectively. The refined values of the hyperfine parameters extracted from these spectra by nonlinear least-squares fitting are listed in **Table 1**. The spectra in **Figures 1(a)-4(a)** were analyzed considering one six-line pattern, with the magnetic hyperfine field (BHF) characteristic to hematite. A small quadrupole-split doublet was added to these fits to account for the presence of ultrafine hematite nanoparticles, with the dimension less than 7 nm.

A second sextet was introduced in the analysis of the Mössbauer spectra in **Figures 1(b)~(e)-4(b)~(e)** with the magnetic hyperfine field smaller than that of hematite and assigned to gadolinium-doped hematite nanoparticles. This sextet originates from substitutions of Fe atoms by Gd atoms and is consistent with the model of local atomic environment. Moreover, a third sextet was necessary in the Mössbauer spectrum of **Figure 1(c)** demonstrating an increased level of the substitutions in the sample milled for 4 h. The dependence of the BHF values of these sextets on the ball milling time is depicted in **Figure 5** and indicates the formation of a limited solid solution in the studied samples. A higher level of

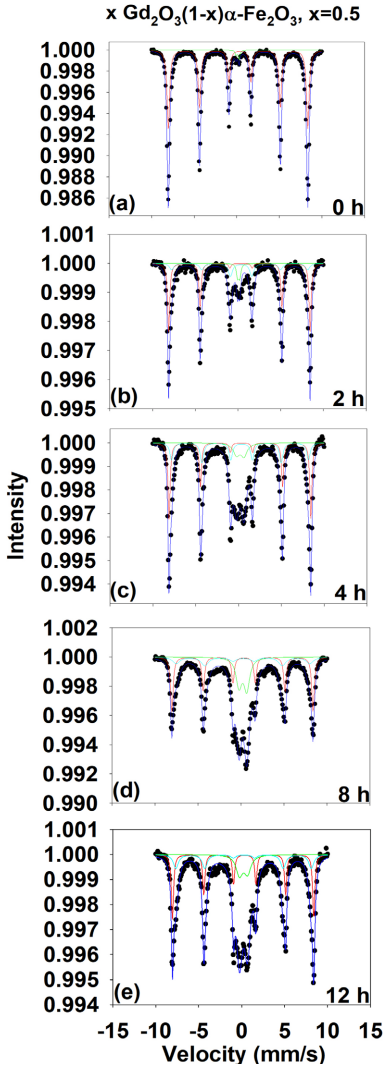

Figure 3. Mössbauer spectra for x = 0.5 at different milling times.

substitution is not possible due to the difference in the ionic radii of the Gd^{3+} ions (0.938 Å) and Fe^{3+} ions (0.645 Å). It may be noted that the formation of a solid solution was not observed in the xNd_2O_3-(1-x)α-Fe_2O_3 system reported previously, due to the specific chemistry of the Nd ions [26].

The Mössbauer spectra in **Figure 1(d)**, **Figure 1(e)** and **Figures 2(b)~(e)-4(b)~(e)** were analyzed by considering an additional quadrupole-split doublet, with the hyperfine parameters (quadrupole splitting QS and isomer shift, IS, relative to Fe) characteristic to the gadolinium perovskite, $GdFeO_3$. **Figure 6** displays the dependence of the relative abundance of this doublet as function of the ball milling time for all values of the molarities used. It can be seen that the contribution of this doublet increases with increasing milling time and reaches 41.64% for the sample with x = 0.7 ball-milled for 12 hours. The occurrence of the gadolinium perovskite can be understood by considering the reaction Gd_2O_3 + Fe_2O_3 → $2GdFeO_3$, which is believed to occur during the mechanochemical activation process.

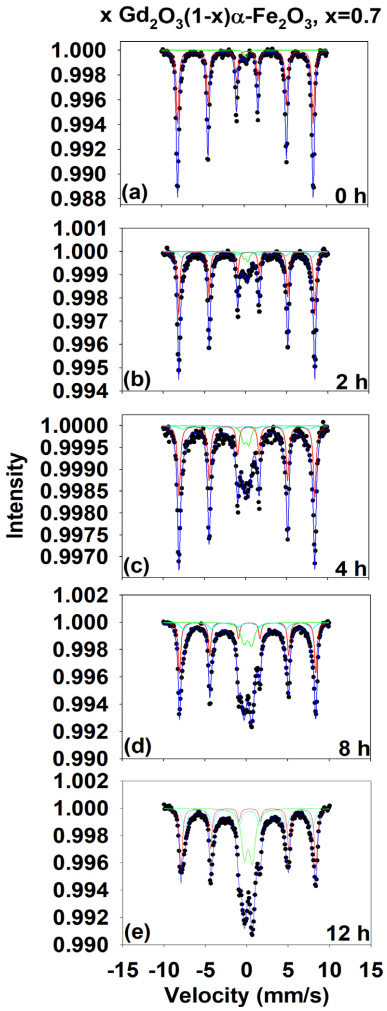

Figure 4. Mössbauer spectra for x = 0.7 at different milling times.

3.2. X-Ray Powder Diffraction (XRPD)

Figures 7(a)-(e) shows the XRPD patterns of the xGd_2O_3-(1-x)α-Fe_2O_3 nanoparticles system for x = 0.5 and ball milling times of 0, 2, 4, 8 and 12 hours, respectively. The pattern in **Figure 7(a)** is consistent with the reflections from α-Fe_2O_3 (PDF card 01-089-0597) and Gd_2O_3 (PDF card 03-065-3181), which represent the starting material. It can be observed that after milling, the reflections indicative of the gadolinium perovskite appear (PDF card 01-074-1900). The lines of $GdFeO_3$ dominate the XRPD pattern after 12 h of exposure to mechanochemical activation. These results are in good, qualitative agreement with the Mössbauer findings presented previously.

3.3. Magnetic Measurements

Figure 8(a) shows the hysteresis curve for the gadolinium oxide-hematite equimolar composition (x = 0.5) at 0 h of milling, recorded at 300 K with a 5 T applied magnetic field. The plot is consistent with the presence of a paramagnetic component specific to Gd_2O_3 (known as a perfect paramagnet) and a weak

Table 1. Hyperfine parameters of the xGd_2O_3-(1-x)α-Fe_2O_3 nanoparticles.

Sample (x)	BMT (h)	I.S, (mm/s)	Q.S. (mm/s)	BHF (T)	Abundance (%)	Phase
0.1	0	0.26	−0.22	50.84	98.75	α-Fe_2O_3
		0.14	0.35		1.23	<7 nm
	2	0.26	−0.21	51.15	65.18	α-Fe_2O_3
		0.26	−0.20	49.65	34.82	Gd:Fe_2O_3
	4	0.26	−0.20	51.4	35.05	α-Fe_2O_3
		0.26	−0.61	50.33	33.25	Gd:Fe_2O_3
		0.26	−0.17	48.27	31.70	Gd:Fe_2O_3
	8	0.27	−0.20	51.00	63.13	α-Fe_2O_3
		0.26	−0.17	48.27	34.45	Gd:Fe_2O_3
		0.10	0.27		2.42	$GdFeO_3$
	12	0.27	−0.20	50.90	44.29	α-Fe_2O_3
		0.26	−0.11	47.30	53.58	Gd:Fe_2O_3
		0.32	0.57		2.13	$GdFeO_3$
0.3	0	0.26	−0.21	50.87	97.55	α-Fe_2O_3
		0.09	0.32		2.45	<7 nm
	2	0.26	−0.20	51.17	68.03	α-Fe_2O_3
		0.25	−0.18	49.01	30.02	Gd:Fe_2O_3
		0.18	0.47		1.95	$GdFeO_3$
	4	0.26	−0.19	51.13	55.51	α-Fe_2O_3
		0.26	−0.22	48.68	35.63	Gd:Fe_2O_3
		0.19	0.72		8.86	$GdFeO_3$
	8	0.26	−0.20	51.03	35.95	α-Fe_2O_3
		0.26	−0.17	48.58	31.91	Gd:Fe_2O_3
		0.21	0.88		32.14	$GdFeO_3$
	12	0.26	−0.20	51.08	31.13	α-Fe_2O_3
		0.20	−0.22	47.33	27.25	Gd:Fe_2O_3
		0.21	0.79		41.62	$GdFeO_3$
0.5	0	0.26	−0.22	50.78	98.26	α-Fe_2O_3
		0.09	0.35		1.74	<7 nm
	2	0.26	−0.18	51.32	50.94	α-Fe_2O_3
		0.28	−0.18	49.35	42.94	Gd:Fe_2O_3
		0.08	0.26		6.12	$GdFeO_3$
	4	0.26	−0.18	51.33	35.26	α-Fe_2O_3

Continued

		0.27	−0.18	49.54	37.04	Gd:Fe_2O_3
		0.20	0.87		27.70	$GdFeO_3$
	8	0.26	−0.19	50.89	27.49	α-Fe_2O_3
		0.26	−0.06	48.13	36.65	Gd:Fe_2O_3
		0.22	0.91		35.86	$GdFeO_3$
	12	0.26	−0.19	51.01	28.15	α-Fe_2O_3
		0.25	−0.05	48.87	34.80	Gd:Fe_2O_3
		0.21	0.94		37.0	$GdFeO_3$
0.7	0	0.26	−0.21	50.95	98.33	α-Fe_2O_3
		0.11	0.32		1.67	<7 nm
	2	0.26	−0.20	51.28	63.19	α-Fe_2O_3
		0.24	−0.18	49.14	28.38	Gd:Fe_2O_3
		0.03	0.52		8.43	$GdFeO_3$
	4	0.26	−0.18	51.18	58.69	α-Fe_2O_3
		0.11	−0.16	47.76	24.47	Gd:Fe_2O_3
		0.10	0.63		16.85	Gd:Fe_2O_3
	8	0.26	−0.19	51.05	32.57	α-Fe_2O_3
		0.24	−0.15	48.26	30.36	Gd:Fe_2O_3
		0.18	0.93		37.06	$GdFeO_3$
	12	0.27	−0.15	50.54	23.94	α-Fe_2O_3
		0.27	−0.06	47.93	34.42	Gd:Fe_2O_3
		0.19	0.96		41.64	$GdFeO_3$
Errors:		±0.01	±0.02	±0.5	±0.5	

ferromagnetic component, due to hematite. The magnetic state of hematite is antiferromagnetic with the Neel temperature T_N = 960 K [1]-[5]. Specific to hematite is the fact that its two magnetic sublattices have equal moment and antiparallel orientation below the Morin temperature, T_M = 262 K, for pure hematite [7]. At temperatures higher than the Morin temperature, the two sublattices are slightly canted, leading to weak ferromagnetism [27]. This phenomenon explains the presence of the coercive field of H_c = 158 Oe.

Figure 8(b) displays the hysteresis loop of the 0-h equimolar sample recorded at 5 K and 5 T. It can be seen that the magnetization varies linearly with the applied magnetic field, dependence due to the paramagnetic behavior of gadolinium oxide and the antiferromagnetic behavior of hematite. The order-of-magnitude increase in the magnetization at 5 K compared to the magnetization at 300 K can be explained by the temperature dependence of magnetization given in **Figure 8(c)**. The magnetization evolution with temperature was measured via the

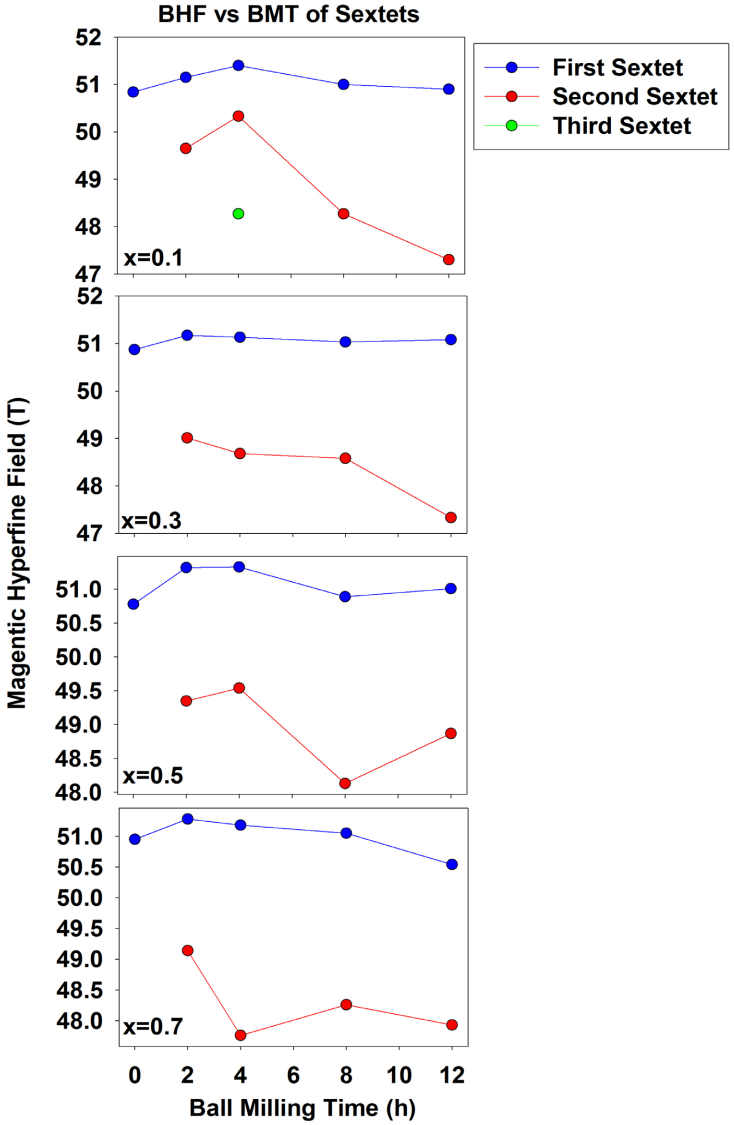

Figure 5. Magnetic hyperfine fields as function of composition and ball-milling time.

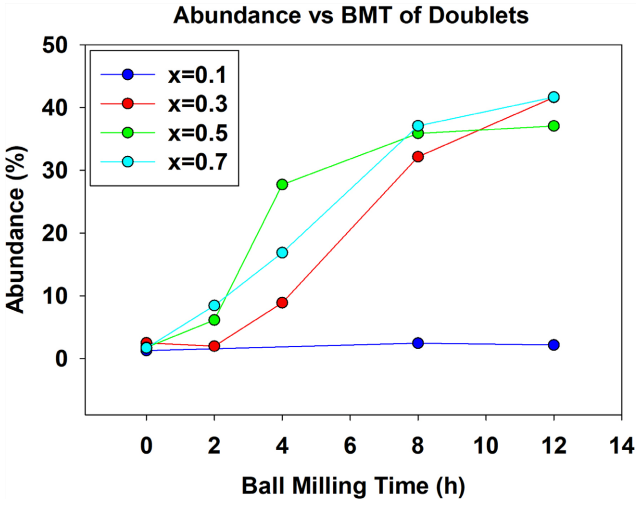

Figure 6. Abundance of doublet as function of ball-milling time.

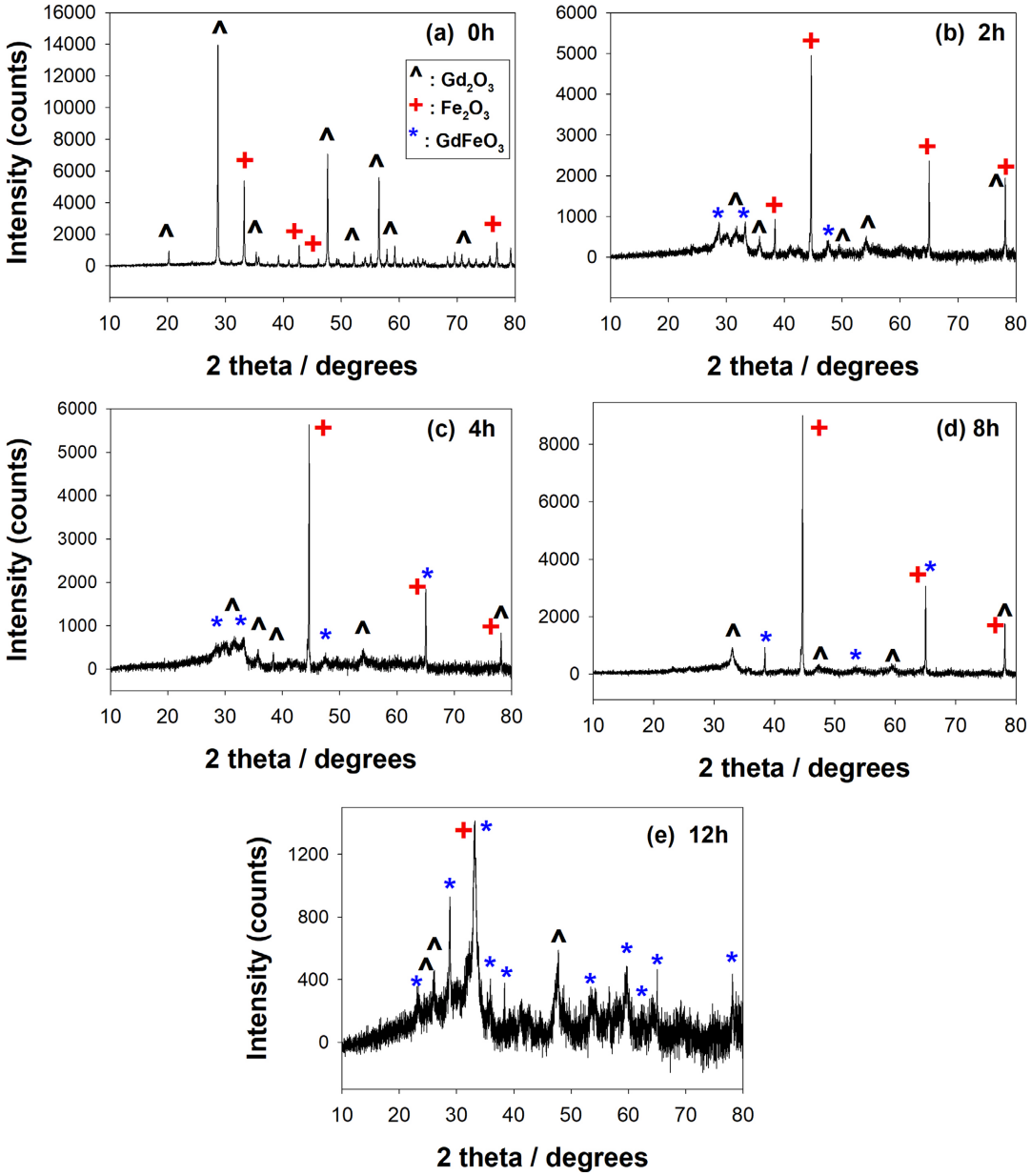

Figure 7. XRPD patterns for the equimolar composition (x = 0.5) as function of BMT.

zero-field-cooling-field cooling (ZFC-FC) procedure: first, the sample was cooled in zero field, then a 200 Oe magnetic field was applied, the ZFC dependence on heating was recorded and next, the temperature dependence of the magnetization on the FC was measured. The thermal hysteresis between 145 and 215 K given by the ZFC-FC curves reveals a first-order thermodynamic transition, which is specific to the Morin transition of hematite. In our case, this transition occurs at lower temperatures, due to the smaller grain sizes and the equimolar mixture of hematite and gadolinium oxide.

It can be seen in **Figure 8(d)** for the 4-h sample that the coercive field evidenced at 300 K significantly decreased, while the magnetization increased, without reaching saturation in a field of 5 T. Further increase in the magnetization

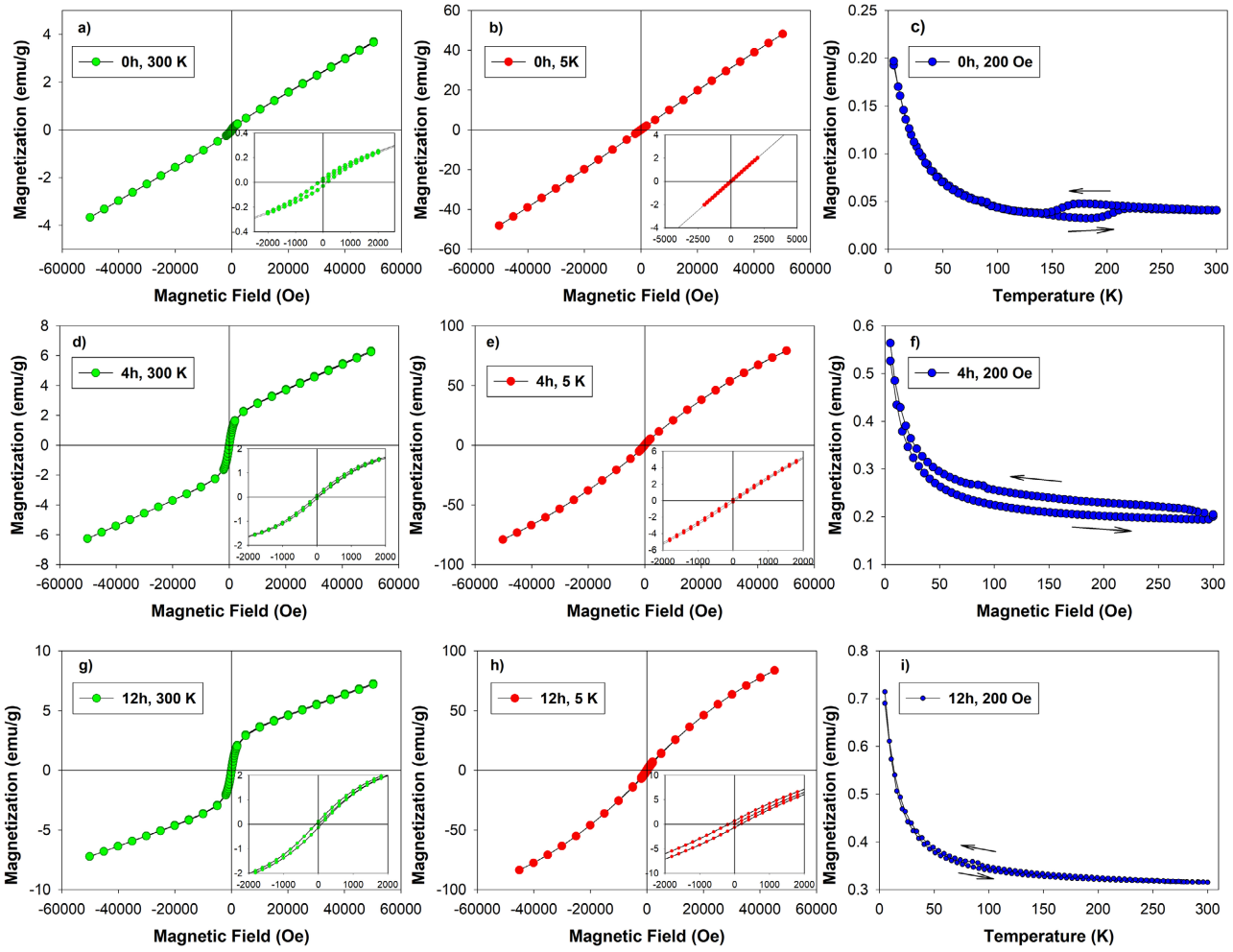

Figure 8. Variation of the hysteresis loops at 300 K (panels (a), (d), (g)) and 5 K (panels (b), (e), (h)) for Gd_2O_3-Fe_2O_3 samples at 0 h and after 4 h and 12 h of ball-milling, respectively. Variation of magnetization as function of temperature at ZFC-FC and 200 Oe, for the initial (panel (c)) and the ball-milled samples at 4 h (panel (f)) and 12 h (panel (i)), respectively.

can be observed in the hysteresis loop recorded at 5 K and depicted in Figure 8(e). As can be inferred from Figure 8(f), the thermal hysteresis specific to the Morin transition is drastically affected after the 4-h milling time. Thus, the Morin transition occurs over a broad temperature range and the antiferromagnetic coupling is replaced by the weak ferromagnetism down to 20 K. This is due to the decrease in the dimension of the nanoparticles formed.

The hysteresis curves recorded for the sample milled for 12 h reveal an increase in magnetization and coercivity both at 300 K (Figure 8(g)) and 5 K (Figure 8(h)). As a result of the ball milling performed, Gd substitutions for Fe in the hematite lattice add increasingly higher contributions to magnetization. The ZFC-FC dependence specific to the 12-h milled sample (Figure 8(i)) shows a small Morin transition, between 60 and 100 K, result which is consistent with the consumption of hematite in the mechanochemical activation reaction and the formation of the gadolinium perovskite phase. In $GdFeO_3$, Gd-Gd, Gd-Fe and Fe-Fe interactions result in its antiferromagnetic behavior along with a weak

ferromagnetic behavior [22] [23]. Consequently, in the equimolar mixture of Gd_2O_3-Fe_2O_3 we deal with a superposition of magnetic behaviors, with multiple magnetic phase transitions for both intrinsic causes and changes induced by mechanical grinding.

3.4. Optical Diffuse Reflectance Spectroscopy

Figure 9(a) shows the optical absorption spectra of the gadolinium oxide-hematite equimolar mixture as function of energy over the UV-VIS-NIR spectral range for all milling times employed. For the starting material, hematite has a band gap of 1.9 - 2.2 eV in the visible region, while gadolinium oxide has a gap value of 5.2 eV in the ultraviolet range. For the ball-milled material, it can be seen that the absorbance is considerably enhanced and broadened, an effect we believe to result from the substitution of Gd ions for Fe.

Since the 2.2 eV transition in hematite is indirect, a plot of $(\alpha E)^2$ as function of energy (eV) is able to yield the band gap of the compound, according to the Tauc plots [28] [29] [30]. Indeed, it can be observed in Figure 9(b)) that the intercepts give a value of ~2.1 eV for the band gap; moreover, this value is independent of

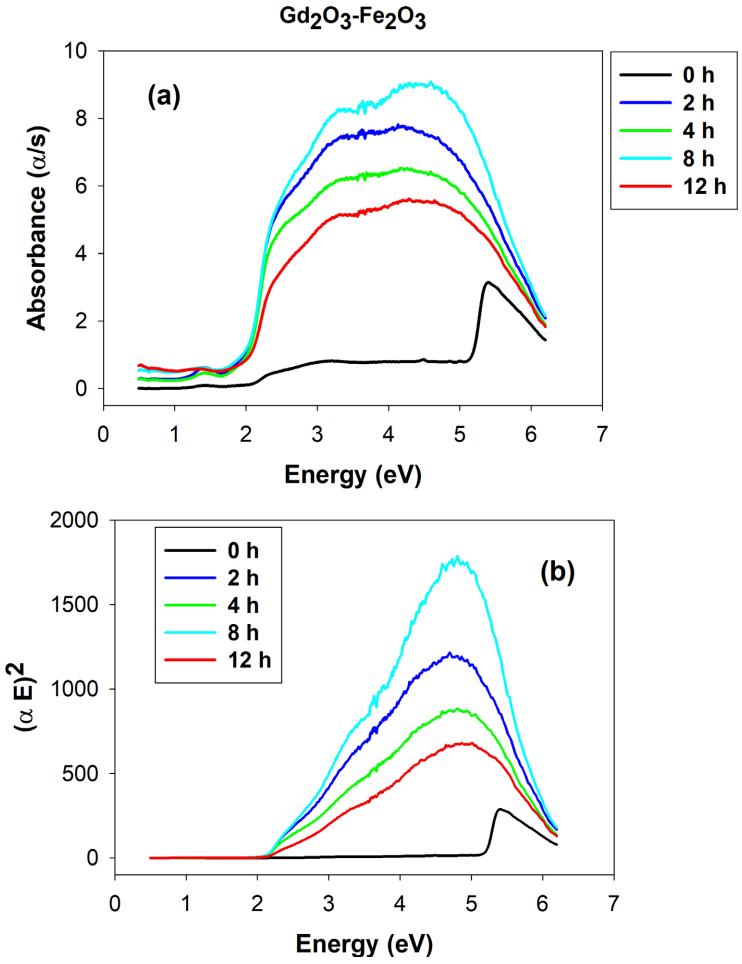

Figure 9. Optical diffuse reflectance spectra for the equimolar composition as function of BMT.

the milling time employed. These results show that the gadolinium oxide-hematite mixed-oxide nanostructures have semiconductor properties.

4. Conclusion

In this study, we successfully synthesized the compositional series xGd_2O_3-$(1-x)\alpha$-Fe_2O_3 at four different molar ratios (x = 0.1, 0.3, 0.5 and 0.7) by mechanochemical activation and characterized its magnetic and optical properties as function of ball milling time by Mössbauer spectroscopy, X-ray powder diffraction, magnetic measurements and optical diffuse reflectance spectroscopy. Both hysteresis loops and zero-field-cooling-field-cooling determinations were employed. It was found that solid solutions were formed and the gadolinium perovskite was the end product of the milling performed. The compounds were semiconductors with band gaps of 2.1 eV. Semiconducting oxides have formed the basis for technological significant advancements in displays, sensors and photovoltaics, and are setting the stage for emerging applications related to mechanically flexible electronics.

Acknowledgements

This work was supported in part by the National Science Foundation, USA under grants number DMR-0854794 and DMR-1002627-1. Funding was also received from the Ministry of Research, Innovation and Digitization (Romania), CNCS/CCCDI-UEFISCDI projects number CPN-III-P2-2.1-PED 493/2020. J.A.A. and A.J.C. acknowledge the support of the National Science Foundation, USA under Grant DMR-1611198. The X-ray powder diffractometer was purchased with funds from the National Science Foundation, USA (DUE-0511444) and an upgrade was financed by the Bayer School of Natural and Environmental Sciences at Duquesne University.

Conflicts of Interest

The authors declare no conflicts of interest regarding the publication of this paper.

References

[1] Iordanova, N., Dupuis, M. and Rosso, K.M. (2005) Charge Transport in Metal Oxides: A Theoretical Study of Hematite α-Fe_2O_3. *Journal of Chemical Physics*, **122**, Article ID: 144305. https://doi.org/10.1063/1.1869492

[2] Rozenberg, G.Kh., Dubrovinsky, L.S., Pasternak, M.P., Naaman, O., LeBihan, T. and Ahuja, R. (2002) High Pressure Structural Studies of Hematite Fe_2O_3. *Physical Review B*, **65**, Article ID: 064112. https://doi.org/10.1103/PhysRevB.65.064112

[3] Bergenmayer, W., Schweiger, H. and Wimmer, E. (2004) *Ab Initio* Thermodynamics of Oxide Surfaces: O_2 on Fe_2O_3 (0001). *Physical Review B*, **69**, Article ID: 195409. https://doi.org/10.1103/PhysRevB.69.195409

[4] Zheng, Y., Cheng, Y., Wang, Y., Bao, F., Zhou, L., Wei, X., Zhang, Y. and Zheng, Q. (2006) Quasicubic α-Fe_2O_3 Nanoparticles with Excellent Catalytic Performance.

Journal of Physical Chemistry, **110**, 3093-3097. https://doi.org/10.1021/jp056617q

[5] Wu, C., Yin, P., Zhu, X., Yang, C.O. and Xie, Y. (2006) Synthesis of Hematite (α-Fe_2O_3) Nanorods: Diameter-Size and Shape Effects on Their Applications in Magnetism, Lithium Ion Battery, and Gas Sensors. *Journal of Physical Chemistry B*, **110**, 17806-17812. https://doi.org/10.1021/jp0633906

[6] Reddy, B.V., Rasouli, F., Hajaligol, M.R. and Khanna, S.N. (2004) Novel Mechanism for Oxidation of CO by Fe_2O_3 Clusters. *Fuel*, **83**, 1537-1541. https://doi.org/10.1016/j.fuel.2003.12.015

[7] Liu, J.Z. (1986) Morin Transition in Hematite Doped with Iridium Ions. *Journal of Magnetism and Magnetic Materials*, **54**-**57**, 901-902. https://doi.org/10.1016/0304-8853(86)90305-7

[8] Sanchez, C., Sieber, K.D. and Somorjai, G.A. (1988) The Photochemistry of Niobium Doped α-Fe_2O_3. *Journal of Electroanalytical Chemistry*, **252**, 269-290. https://doi.org/10.1016/0022-0728(88)80216-X

[9] Oliveira, L.C.A., Zaera, F., Lee, I., Lima, D.Q., Ramalho, T.C., Silva, A.C. and Fonseca, E.M.B. (2009) Nb-Doped Hematites for Decomposition of Isopropanol: Evidence of Surface Reactivity by *In-Situ* CO Adsorption. *Applied Catalysis A*, **368**, 17-21. https://doi.org/10.1016/j.apcata.2009.08.001

[10] Tilley, S.D., Cornuz, M., Sivula, K. and Gratzel, M. (2010) Light-Induced Water Splitting with Hematite: Improved Nanostructure and Iridium Oxide Catalysis. *Angewandte Chemie*, **49**, 6405-6408. https://doi.org/10.1002/anie.201003110

[11] Kleiman-Shwarsctein, A., Huda, M.N., Walsh, A., Yan, Y., Stucky, G.D., Hu, Y.S., Al-Jassim, M.M. and McFarland, E.W. (2010) Electrodeposited Aluminum-Doped α-Fe_2O_3 Photoelectrodes: Experiment and Theory. *Chemistry of Materials*, **22**, 510-517. https://doi.org/10.1021/cm903135j

[12] Glasscock, J.A., Barnes, P.R.F., Plumb, I.C. and Savvides, N. (2007) Enhancement of Photoelectrochemical Hydrogen Production from Hematite Thin Films by Introduction of Ti and Si. *Journal of Physical Chemistry*, **111**, 16477-16488. https://doi.org/10.1021/jp074556l

[13] Music, S., Ilakovac, V., Ristic, M. and Popovic, S. (1992) Formation of Oxide Phases in the System Fe_2O_3-Gd_2O_3. *Journal of Materials Science*, **27**, 1011-1015. https://doi.org/10.1007/BF01197655

[14] Music, S., Popovic, S., Czako-Nagy, I. and Gashi, F. (1993) Formation of Oxide Phases in the System Fe_2O_3-Gd_2O_3 Part II. *Journal of Materials Science*, **12**, 869-873. https://doi.org/10.1007/BF00278001

[15] Salikhov, S.V., Toleukhanova, S.K., Bordyuzhin, I.G. and Savchenko, A.G. (2019) Phase Composition and Magnetic Properties of Fe_2O_3-FeO-Gd_2O_3 Powders after High-Energy Ball Milling and Thermal Treatment. *Bulletin of the Russian Academy of Sciences*: *Physics*, **83**, 1275-1281. https://doi.org/10.3103/S1062873819100186

[16] Bandyopadhyay, A., Sharma, S., Nath, M., Karmakar, A., Kumari, K. and Sutradhar S. (2021) Dielectric Study and Magnetic Property Analysis of Gd_2O_3 Nanorods/Nanowire in Combination with Monte Carlo Simulation. *Journal of Alloys and Compounds*, **882**, Article ID: 160720. https://doi.org/10.1016/j.jallcom.2021.160720

[17] Patel, S.K.S., Dhak, P., Kim, M.K., Lee, J.H., Kim, M. and Kim, S.K. (2016) Structural and Magnetic Properties of Co-Doped Gd_2O_3 Nanorods. *Journal of Magnetism and Magnetic Materials*, **403**, 155-160. https://doi.org/10.1016/j.jmmm.2015.11.093

[18] Osaka, T., Takahashi, H., Sagayama, H., Yamasaki, Y. and Ishiwata, S. (2017) High-Pressure Synthesis of an Unusual Antiferromagnetic Metal $CaCoO_3$ with $GdFeO_3$-Type Perovskite Structure. *Physical Review B*, **95**, Article ID: 224440.

https://doi.org/10.1103/PhysRevB.95.224440

[19] Paul, R., Sen, P. and Das, I. (2016) Effect of Morphology on the Magnetic Properties of Gd_2O_3 Nanotubes. *Physica E*, **80**, 149-154. https://doi.org/10.1016/j.physe.2016.01.038

[20] Ruffo, A., Mozzati, M.C., Albini, B., Galinetto, P. and Bini, M. (2020) Role of Non-Magnetic Dopants (Ca, Mg) in $GdFeO_3$ Perovskite Nanoparticles Obtained by Different Synthetic Methods: Structural, Morphological and Magnetic Properties. *Journal of Materials Science*: *Materials in Electronics*, **31**, 18263-18277. https://doi.org/10.1007/s10854-020-04374-8

[21] Shah, J. and Kotnala, R.K. (2012) Room Temperature Magnetoelectric Coupling Enhancement in Mg-Substituted Polycrystalline $GdFeO_3$. *Scripta Materialia*, **67**, 316-319. https://doi.org/10.1016/j.scriptamat.2012.05.003

[22] Wu, A., Wang, Z., Wang, B., Ban, X., Jiang, L., Xu, J., Yuan, S. and Cao, S. (2014) Crystal Growth and Magnetic Properties of $GdFeO_3$ Crystals by Floating Zone Method. *Solid State Communications*, **185**, 14-17. https://doi.org/10.1016/j.ssc.2014.01.011

[23] Vandana, C.S. and Rudramadevi, B.H. (2019) Structural, Magnetic and Dielectric Properties of Cobalt Doped $GdFeO_3$ Orthoferrites. *Materials Research Express*, **6**, Article ID: 126126. https://doi.org/10.1088/2053-1591/ab768f

[24] Paul, P., Prajapat, C.L., Rajarajan, A.K. and Chandrasekhar Rao, T.V. (2018) Low Temperature Magnetic Properties of $GdFeO_3$. *AIP Conference Proceedings*, **1942**, Article ID: 130029. https://doi.org/10.1063/1.5029099

[25] Zhu, X.H., Xiao, X.B., Chen, X.R. and Liu, B.G. (2017) Electronic Structure, Magnetism and Optical Properties of Orthorhombic $GdFeO_3$ from First Principles. *RSC Advances*, **7**, 4054. https://doi.org/10.1039/C6RA25259A

[26] Sorescu, M., Diamandescu, L., Sofronie, M., Pratt, C. and Jubeck, J. (2022) Mechanochemical Synthesis and Mössbauer Characterization of Neodymium Oxide-Hematite Magnetic Ceramic Nanoparticles: Phase Sequence and Recoilless Fraction. *Materials Chemistry and Physics*, **277**, Article ID: 125511. https://doi.org/10.1016/j.matchemphys.2021.125511

[27] Stroh, C., Tolea, F., Valeanu, M., Diamandescu, L., Xu, T. and Sorescu, M. (2015) Ruthenium Oxide-Hematite Magnetic Ceramics Nanostructures. *Ceramics International*, **41**, 14367-14375. https://doi.org/10.1016/j.ceramint.2015.07.070

[28] Tauc, J., Grigorovici, R. and Vancu, A. (1966) Optical Properties and Electronic Structure of Amorphous Germanium. *Physica Status Solidi*, **15**, 627. https://doi.org/10.1002/pssb.19660150224

[29] Mallick, P. and Dash, B.N. (2013) X-Ray Diffraction and UV-Visible Characterizations of α-Fe_2O_3 Nanoparticles Annealed at Different Temperature. *Nanoscience and Nanotechnology*, **3**, 130-134.

[30] Hussain, Z. (2021) Optical Band Gap, Oxidation Polarizability, Optical Basicity and Electronegativity Measurements of Silicate Glasses Using Ellipsometer and Abbe Refractometer. *New Journal of Glass and Ceramics*, **11**, 1-33. https://doi.org/10.4236/njgc.2021.111001